Inelastic Neutron Scattering and Optical Spectroscopy of Dy^{3+} Single Ions and Dimers in $Cs_3Y_2Br_9$:10% Dy^{3+} and $Cs_3Dy_2Br_9$

M. A. Aebersold,† H. U. Güdel,*,† A. Furrer,‡ and H. Blank§

Institut für Anorganische Chemie, Universität Bern, CH-3000 Bern 9, Switzerland, Laboratorium für Neutronenstreuung, ETH Zürich, CH-5232 Villigen PSI, Switzerland, and Institut Laue-Langevin, 38042 Grenoble Cedex, France

Received July 8, 1993⊛

Dy^{3+} single ions in $Cs_3Y_2Br_9$ and Dy^{3+}–Dy^{3+} dimers in $Cs_3Dy_2Br_9$ were studied by optical spectroscopy and by inelastic neutron scattering (INS). In the diluted compound the energy level scheme for the eight crystal electric field (CEF) levels of the $^6H_{15/2}$ ground-state multiplet of Dy^{3+} in C_{3v} symmetry is obtained and the CEF parameters are determined. In neat $Cs_3Dy_2Br_9$ the effect of exchange interactions can directly be observed, both by optical and INS spectroscopy. The ground and first excited CEF levels are further split due to the exchange interaction between the two Dy^{3+} ions. These splittings can be accounted for by a Heisenberg Hamiltonian with an antiferromagnetic exchange parameter $2J = -0.05$ cm^{-1}.

1. Introduction

Designing magnetic molecular materials has become a subject of great interest in the past years, and new magnetic compounds have been synthesized and investigated using various experimental techniques such as magnetic susceptibility and heat capacity measurements, EPR, optical spectroscopy, and inelastic neutron scattering (INS).[1] In order to understand the basics of exchange interactions, small clusters and especially dimers have shown to be ideal model systems. Many exchange-coupled transition metal (TM) dimers have been investigated in the past.[2,3] Dimers of rare earth (R) ions, on the other hand, have received less attention until recently.[4,5] Due to the well-shielded f-electrons the exchange interactions are small and very sensitive techniques have to be used to study R dimers. INS spectroscopy has proven to be a powerful tool for such investigations.[4] Transitions between the lowest crystal electric field (CEF) levels of R ions as well as exchange splittings can directly be observed. The detailed analysis of the INS intensities as a function of the modulus of the scattering vector Q provides detailed information about the wave functions of the dimers and thus about the anisotropy of the exchange.[6] Exchange interactions also affect the optical spectroscopic properties. Besides the energy splittings of the CEF levels, they can lead to cooperative excitations and energy-transfer phenomena such as cross-relaxation and up-conversion.[5]

A model system for such studies is the family of compounds $Cs_3R_2Br_9$ (R = Sm^{3+}–Lu^{3+}, Y^{3+}). They crystallize in the space group $R\bar{3}c$ and contain $R_2Br_9^{3-}$ dimers consisting of two face-sharing RBr_6^{3-} octahedra as discrete units.[7] The dimer point symmetry is approximately D_{3h} (the actual symmetry is C_3), and the 3-fold dimer axis coincides with the crystal c axis.

INS experiments on $Cs_3Tb_2Br_9$ showed that, for the Tb^{3+}–Tb^{3+} dimers, a Heisenberg–Dirac–Van Vleck (HDVV) type of exchange was adequate to describe the observed splittings in the ground and first excited CEF level.[8] For Yb^{3+}–Yb^{3+} dimers in $Cs_3Yb_2Br_9$ a HDVV Hamiltonian with effective spins $S_{Yb} = 1/2$ satisfactorily explained the observed singlet–triplet splitting within the ground CEF level,[4] and only with high-resolution INS spectra could a small exchange anisotropy be detected.[9] For Ho^{3+}–Ho^{3+} dimers, on the other hand, anisotropy was found to be important and an exchange-tensor formalism was used to account for the energy splittings of the three lowest CEF levels and the INS intensities.[10] Detailed information about CEF splittings and exchange interactions up to about 15 cm^{-1} was obtained for all these dimers. Simplified models assuming effective spins were used for their analysis. However, for R ions with low-lying excited CEF levels the whole ground-state multiplet has to be taken into account for a detailed analysis.[6] The overall CEF splittings are usually of the order of 400 cm^{-1}, and optical spectroscopy has been shown to be an appropriate technique to determine these splittings.[11]

In the present study we used optical spectroscopy and INS experiments for the investigation of Dy^{3+} single ions in $Cs_3Y_2Br_9$ and Dy^{3+}–Dy^{3+} dimers in the neat $Cs_3Dy_2Br_9$. The CEF splitting of the $^6H_{15/2}$ ground state can be determined from a combination of luminescence and INS spectroscopy. Further splittings due to the exchange interactions can also be probed by both methods. The two experimental techniques are complementary, and their agreement is excellent.

2. Experimental Section

(a) Synthesis. Polycrystalline samples of $Cs_3Dy_2Br_9$ as well as the doped $Cs_3Y_2Br_9$:10% Dy^{3+} were obtained by a slight modification of the general procedure given in ref 12. CsBr (suprapur, Merck), Y_2O_3 (puriss 99.9%, Fluka), Dy_2O_3 (puriss 99.9%, Fluka) and HBr (47%, suprapur, Merck) were used as starting materials. The HBr (purity >99.8%, Fluka) gas-flow treatment to dry the intermediate product was carried out at 510 °C. Single crystals were grown by the Bridgman technique at 850 and 700 °C for neat and doped samples, respectively, with a growth rate of 0.03 mm/min. All samples were checked by powder X-ray diffraction. Due to their hygroscopic character they had to be handled under a dry inert atmosphere.

* To whom correspondence should be addressed.
† Universität Bern.
‡ ETH Zürich.
§ Institut Laue-Langevin.
⊛ Abstract published in *Advance ACS Abstracts*, February 1, 1994.

(1) Gatteschi, D., Kahn, O., Miller, J. S., Palacio, F., Eds.; *Magnetic Molecular Materials*; NATO ASI Series Vol. 198; Kluwer: Dordrecht, The Netherlands, 1991; Vol. 198.
(2) Bencini, A.; Gatteschi, D. *EPR of Exchange Coupled Systems*; Springer: Berlin, 1990.
(3) McCarthy, P. J.; Güdel, H. U. *Coord. Chem. Rev.* **1988**, *88*, 69.
(4) Güdel, H. U.; Furrer, A.; Blank, H. *Inorg. Chem.* **1990**, *29*, 4081.
(5) Hehlen, M. P.; Güdel, H. U. *J. Chem. Phys.* **1993**, *98*, 1768.
(6) Aebersold, M. A.; Güdel, H. U.; Hauser, A.; Furrer, A.; Blank, H.; Kahn, R. *Phys. Rev. B* **1993**, *48*, 12723.
(7) Meyer, G.; Schönemund, A. *Mater. Res. Bull.* **1980**, *15*, 89.
(8) Furrer, A.; Güdel, H. U.; Blank, H.; Heidemann, A. *Phys. Rev. Lett.* **1989**, *62*, 210.
(9) Aebersold, M. A.; Güdel, H. U.; Hauser, A.; Furrer, A.; Guillaume, M.; Carlile, C. J. Work in progress.
(10) Furrer, A.; Güdel, H. U.; Krausz, E. R.; Blank, H. *Phys. Rev. Lett.* **1990**, *64*, 68.
(11) Richardson, F. S.; Reid, M. F.; Dallara, J. J.; Smith, R. D. *J. Chem. Phys.* **1985**, *83*, 3813.
(12) Meyer, G. *Inorganic Syntheses*; Holt, S. L., Ed.; Wiley: New York, 1983; Vol. 22.

0020-1669/94/1333-1133$04.50/0

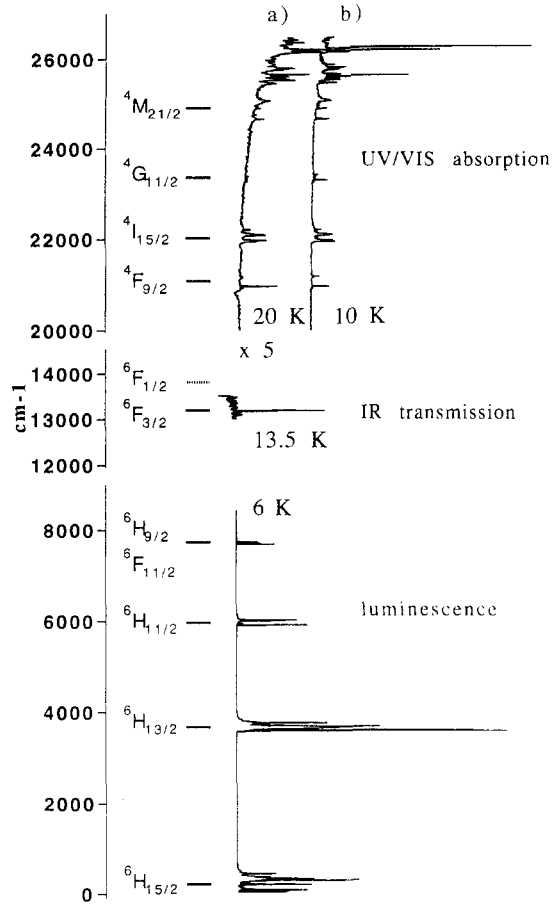

Figure 1. Trace a: UV/vis absorption, IR transmission, and luminescence spectra under excitation of the $^6H_{15/2}$ (0) → $^4F_{9/2}$ (2′) transition at 20 960 cm^{-1} of $Cs_3Y_2Br_9$:10% Dy^{3+}. Trace b: UV/vis absorption spectrum of $Cs_3Dy_2Br_9$.

(b) Optical Spectroscopy. For single-crystal absorption and transmission spectroscopy the light of an Oriel 100-W tungsten lamp, dispersed by two gratings (1200 grooves/mm, blazed at 500 nm) in a 0.85-m double monochromator (Spex 1402), was used as a light source. The crystal orientation was random, and the light was not polarized. For the single-beam transmission spectra the light was detected by a cooled end window Hamamatsu R 3310 photomultiplier (PM) tube which was connected via a Hamamatsu C716 preamplifier to a Stanford Research SR 400 photon-counting system. For the absorption measurements the light was dispersed by a 0.85-m Spex double monochromator (Spex 1402), split into reference and sample beams by a home built double beam attachment, detected by an EMI 9781A side window PM tube connected to a Keithley 417 picoammeter, and converted to absorbance.

For luminescence and excitation measurements a dye laser (Lambda Physik Fl3002; Coumarin 102 in methanol) pumped by the 3rd harmonic (355 nm) of a pulsed Nd:YAG laser (Quanta Ray DCR-3, 20 Hz) was used. The sample luminescence was dispersed by two gratings (1200 grooves/mm, blazed at 500 nm) in a 0.85-m double monochromator (Spex 1402) and detected by a cooled end window PM (RCA 31034) connected to a photon-counting system (Stanford Research SR 440).

Instrument control and data acquisition were performed by a 286 DOS computer.

Sample cooling was achieved using the helium-gas flow technique.

(c) INS Experiments. The INS experiments were performed on polycristalline samples using the time-of-flight IN5 spectrometer at the Institut Laue-Langevin, Grenoble, France. Due to the high-absorption cross section of Dy a sample thickness of 2 mm was chosen; the other two dimensions of the platelike aluminum container were 40 and 45 mm. The instrument was used with the wavelengths of the incoming neutrons set to 4.8 Å (28.6 cm^{-1}) and 8 Å (10.3 cm^{-1}) giving rise to resolutions of 1 and 0.2 cm^{-1}, respectively.

3. Results

Figure 1 shows low-temperature absorption, transmission, and luminescence spectra of $Cs_3Y_2Br_9$:10% Dy^{3+} (trace a) and an absorption spectrum of $Cs_3Dy_2Br_9$ (trace b). Dy^{3+} has no excited states between $^6F_{1/2}$ around 14 000 cm^{-1} and $^4F_{9/2}$ at 21 000 cm^{-1}, and no transitions were observed in this range. This large energy gap is responsible for the long lifetime of the $^4F_{9/2}$ state and, as a result, for the observed luminescences from this state. As in $Cs_2NaDyCl_6$ the transition $^6H_{15/2}$ → $^6F_{1/2}$ was not observed in absorption.[11] From the luminescence spectrum the energies and splittings of all the states up to 8000 cm^{-1} are obtained (Figure 1). In neat $Cs_3Dy_2Br_9$ the luminescence is totally quenched. Above $^4M_{21/2}$ the energy states of Dy^{3+} are lying close together and we do not attempt to make any assignments. The differences of the spectra of Dy^{3+} single ions and dimers are very small as can be seen by comparing the trace a and b of Figure 1 in the UV/vis region. In the present work we concentrate on three states: $^4F_{9/2}$ from which the luminescence is observed, $^6F_{3/2}$, and the $^6H_{15/2}$ ground state.

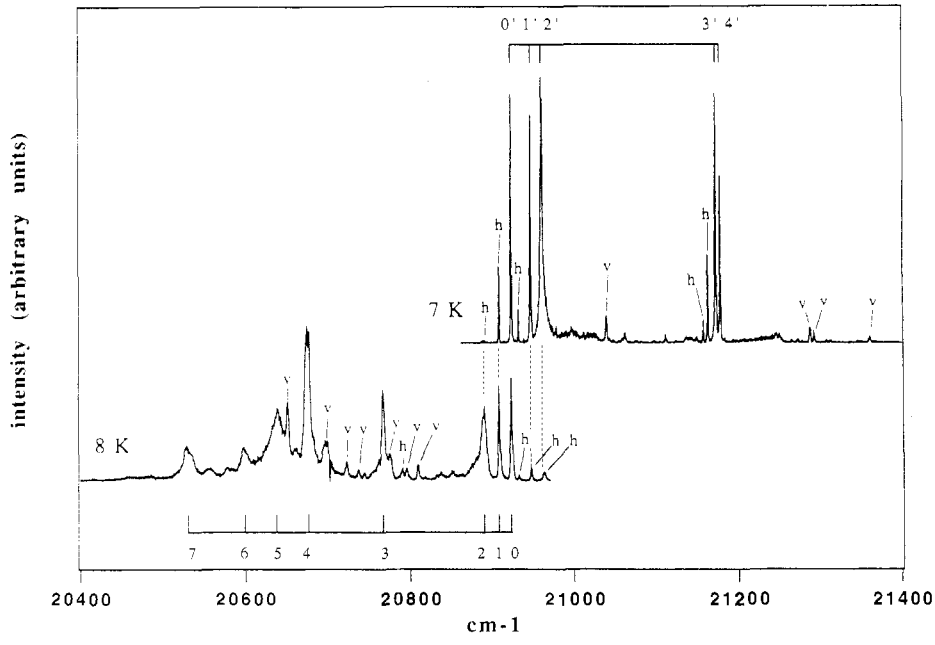

Figure 2. Excitation (top trace) and luminescence (bottom trace) spectra of $Cs_3Y_2Br_9$:10% Dy^{3+}. Excitation: The $^4F_{9/2}$ region is monitored, and the $^4F_{9/2}$ (0′) → $^6H_{15/2}$ (7) transition at 20531 cm^{-1} is detected. Luminescence: Excitation of the $^6H_{15/2}$ (0) → $^4F_{9/2}$ (2′) transition at 20 960 cm^{-1}.

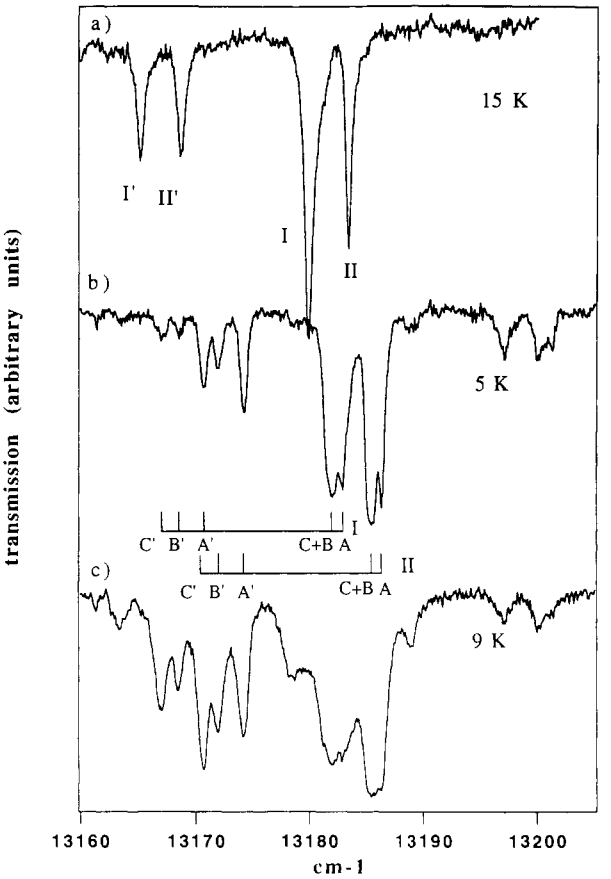

Figure 3. Transmission spectra in the $^6F_{3/2}$ region of $Cs_3Y_2Br_9$:10% Dy^{3+} (trace a) and of $Cs_3Dy_2Br_9$ for two temperatures (traces b and c).

The upper trace of Figure 2 shows the excitation spectrum of the $^4F_{9/2} \rightarrow {}^6H_{15/2}$ luminescence (detected at 20 531 cm^{-1}) for $Cs_3Y_2Br_9$:10% Dy^{3+} at 7 K. The five most prominent bands are centered at 20 923, 20 947, 20 960, 21 172, and 21 178 cm^{-1} and labeled 0′, 1′, 2′, 3′, and 4′, respectively. They are also observed in absorption, for both Dy^{3+} single ions and dimers (shifted by a few wavenumbers in the dimer spectra). There are several weaker bands shifted to lower energy by 15 and 33 cm^{-1}, respectively, compared to the five prominent bands. Their intensities increase with increasing temperature. These "hot" bands are labeled h in Figure 2. At 80 K additional hot bands appear at energies shifted by 156 and 250 cm^{-1}, respectively. Two series of sidebands are observed at higher energies compared to the five bands 0′–4′. The most prominent bands are labeled v. One set is shifted by 115 cm^{-1}, and the second one, by 189 cm^{-1}. The intensity of these bands decreases with increasing temperature, and they can therefore clearly by distinguished from the hot bands. The same excitation spectrum was obtained by detecting other luminescence transitions.

The bottom trace of Figure 2 shows the $^4F_{9/2} \rightarrow {}^6H_{15/2}$ luminescence spectrum of $Cs_3Y_2Br_9$:10% Dy^{3+} at 8 K. The most prominent bands are labeled 0–7. Hot bands shifted to higher energies by 23 and 37 cm^{-1}, respectively, and labeled h are observed. Two sets of "cold" sidebands are shifted to lower energies by 113 and 189 cm^{-1}, respectively, from the bands 0–7. They are labeled v in Figure 2.

Figure 3a shows the $^6H_{15/2} \rightarrow {}^6F_{3/2}$ transmission spectrum of $Cs_3Y_2Br_9$:10% Dy^{3+} under the highest resolution at 15 K. The intensity of the two bands labeled I and II at 13 180 and 13 183 cm^{-1}, respectively, decreases with increasing temperature. The two bands labeled I′ and II′, respectively, are shifted to lower energy by 15 cm^{-1}, and their intensity increases with increasing temperature. They are thus identified as hot bands.

Figure 3b,c shows the same region for the neat $Cs_3Dy_2Br_9$ crystal at 5 and 9 K. The cold transitions are slightly shifted to higher energies compared to Figure 3a. In addition we observe a splitting of the transitions I and II. The splittings are about 1 cm^{-1} with a sharp band labeled A and a broader band labeled B + C at lower energy. There are two series of hot bands with identical energy spacings in the region between 13 165 and 13 180 cm^{-1}; they are labeled I A′–C′ and II A′–C′, respectively. Very similar differences between single ion and dimer absorption spectra are observed for the $^6H_{15/2} \rightarrow {}^4F_{9/2}$ transitions. The splittings of the cold origins in the pair spectra look exactly the same as in Figure 3b. The weak broad bands at higher energies around 13 195 and 12 205 cm^{-1} are not observed in the spectrum of the single ions and can be assigned to cooperative excitations of two neighboring Dy^{3+} ions.

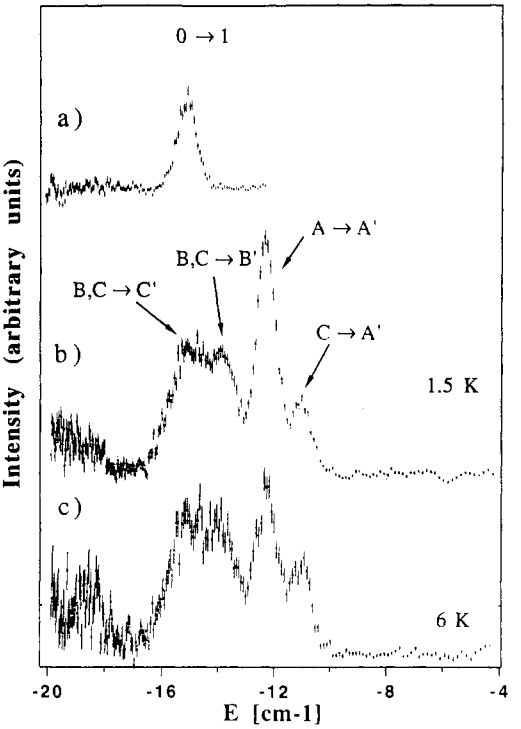

Figure 4. Energy spectra of neutrons scattered from polycrystalline $Cs_3Y_2Br_9$:10% Dy^{3+} (trace a) and $Cs_3Dy_2Br_9$ (traces b and c) (instrument IN5, ILL Grenoble; λ = 4.8 Å).

Figure 4a shows an inelastic neutron scattering spectrum of polycrystalline $Cs_3Y_2Br_9$:10% Dy^{3+} at 2 K. There is one peak centered at 15 cm^{-1}. Figure 4b,c shows the spectra of neutrons scattered from polycrystalline $Cs_3Dy_2Br_9$ at 1.5 and 6 K. As in the transmission experiments, the effect of the exchange coupling is nicely demonstrated. The 0 → 1 transition of Figure 4a is shifted to lower energy and split into several components with a total energy spread of 4 cm^{-1}. We ascribe the bigger CEF splitting in the host lattice to the slightly smaller ionic radius of Y^{3+} ions, thus creating a slightly stronger crystal field. The intensity of the prominent band A → A′ at 12.2 cm^{-1} in Figure 4b,c clearly decreases with increasing temperature. The remaining bands in Figure 4b,c show a slight increase with temperature.

Figure 5 shows the low-energy part of the INS spectrum at 1.8 and 6 K measured with the highest instrumental resolution. The left-hand side of the spectrum, the energy-loss side, corresponds to the excitation of the sample by the neutron beam, and the right-hand side, to energy-gain processes. There is a band centered at ±0.65 cm^{-1}. It is broadened compared to the instrumental resolution. The intensity of the energy-loss peak clearly decreases between 1.8 and 6 K, whereas the intensity of the energy-gain peak increases; see also Table 1. The intensity of this transition as a function of the modulus of the scattering vector Q is shown in Table 2. It is strongly Q dependent, decreasing with decreasing Q. Below Q = 0.4 $Å^{-1}$ it is not observable.

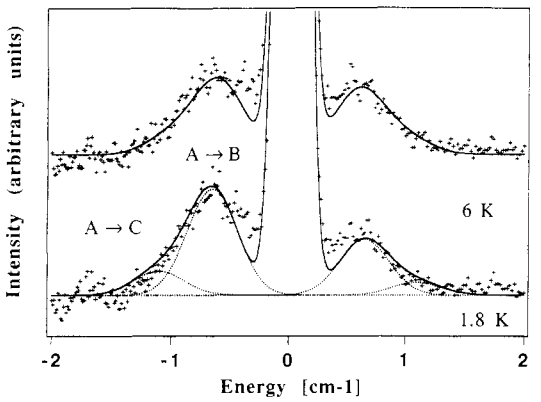

Figure 5. Energy spectra of neutrons scattered from polycrystalline $Cs_3Dy_2Br_9$ for the total of all scattering angles (mean Q = 0.7 Å^{-1}) (instrument IN5, ILL Grenoble; λ = 8.0 Å). The dotted lines were calculated as explained in section 4.2. The full lines are the sum of the individual transitions.

Table 1. Experimental and Calculated Temperature Dependences of the INS Transition at ±0.65 cm^{-1} [a]

	exptl		calcd	
T (K)	loss	gain	loss	gain
1.7	3.0 ± 0.1	1.6 ± 0.1	3.1	1.6
6.0	2.2 ± 0.1	1.7 ± 0.1	2.1	1.7

[a] For the calculation the energies and degeneracies shown in Figure 7c were used. One scaling factor was refined in a least-squares fit of the calculation to the data.

Table 2. Experimental and Calculated Intensity of the INS Transition at ±0.65 cm^{-1} as a Function of the Modulus of the Scattering Vector Q[a]

Q (Å^{-1})	exptl	calcd
0.11	0 ± 0.2	0
0.41	0 ± 0.2	0.3
0.73	0.6 ± 0.2	0.7
1.04	1.0 ± 0.2	0.9

[a] For the experimental intensity the mean value of the energy loss and energy gain transitions at 1.7 and 6 K was taken. For the calculation eq 6 was used. One scaling factor was refined in a least-squares fit of the calculation to the data.

4. Data Analysis and Discussion

4.1. Crystal Field Splittings. Dy^{3+} is a Kramers ion with a $4f^9$ configuration and a $^6H_{15/2}$ free-ion ground-state multiplet. Due to the CEF the $(2J + 1)$-fold degeneracies of the free ion states are lifted in a crystal. For Dy^{3+} in $Cs_2NaDyCl_6$ (O_h-symmetry) most of the CEF levels up to 30 000 cm^{-1} have been located and assigned by Richardson et al.[11] For Dy^{3+} in $Cs_3Y_2Br_9$ and $Cs_3Dy_2Br_9$ the single-ion point symmetry is lowered to C_{3v} and the CEF levels are further split into totally $(2J + 1)/2$ Kramers doublets.

The analysis of the excitation spectrum of Figure 2 is therefore straightforward. The five cold bands labeled 0′–4′ can be assigned to electronic origins of the transitions from the lowest CEF level of the $^6H_{15/2}$ multiplet to the five CEF levels of $^4F_{9/2}$. The hot bands correspond to electronic transitions from excited CEF levels of $^6H_{15/2}$. As expected, there is exact coincidence of the lowest-energy hot bands with the electronic origins observed in emission (lower trace). Similarly, the luminescence spectrum of Figure 2 is used to derive the CEF splitting of $^6H_{15/2}$. The prominent cold bands labeled 0–7 are assigned to electronic origins of the transitions from the 0′ level of $^4F_{9/2}$ to the eight CEF levels of the $^6H_{15/2}$. The hot bands correspond to transitions originating in the 1′ and 2′ levels of $^4F_{9/2}$. The empirical energy level splittings of the $^6H_{15/2}$ and $^4F_{9/2}$ states in a trigonal CEF field thus obtained are shown in Figure 6. The observed transitions are indicated by arrows.

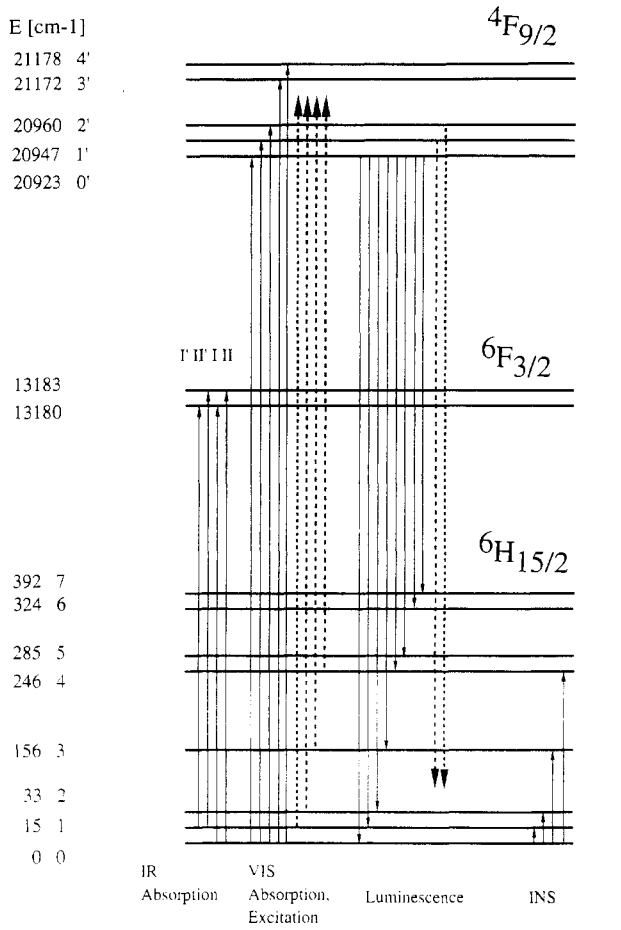

Figure 6. Empirical CEF energy-level scheme for the three states $^4F_{9/2}$, $^6F_{3/2}$, and $^6H_{15/2}$. The transitions observed in the transmission, excitation, luminescence, and INS experiments are indicated by arrows. The broken arrows indicate transitions from one CEF level of the initial state to all CEF components of the final state.

We assign the set of cold sidebands shifted by 189 cm^{-1} in the excitation and luminescence spectra to the totally symmetric stretching mode of the $Dy_2Br_9^{3-}$ unit. From the Raman spectrum of the closely related $Cs_3Yb_2Br_9$ a value of 190 cm^{-1} was obtained for the highest-energy vibration.[5] As in our spectra, a set of sidebands shifted by 113 cm^{-1} was also observed in $Cs_3Yb_2Br_9$;[5] it is most likely due to a bending mode.

The $^6F_{3/2}$ state is split into two CEF levels separated by 3 cm^{-1}. This is a straightforward conclusion from Figure 3, and the result is included in Figure 6.

Finally, the INS transition observed at 15 cm^{-1} in Figure 4a corresponds to the 0 → 1 CEF excitation within the $^6H_{15/2}$ ground state. Other CEF excitations observed by INS but not shown here are included as arrows in Figure 6.

As shown in Table 3, the CEF splittings of $^6H_{15/2}$, $^6F_{3/2}$, and $^4F_{9/2}$ derived from the various techniques are in very good agreement. The sizes of the overall CEF splittings of 392 and 255 cm^{-1} for the $^6H_{15/2}$ and $^4F_{9/2}$ multiplets, respectively, are of the same order as the corresponding splittings of 399 and 288 cm^{-1} found for $Cs_2NaDyCl_6$.[11]

We have calculated the CEF splitting of the $^6H_{15/2}$ ground state. An effective Hamiltonian describing the trigonal CEF interaction for a R ion within a given manifold of angular momentum J can be expressed as[13]

$$\mathbf{H}_{C_{3v}} = B_2\mathbf{O}_2^0 - {}^2/_3B_4(\mathbf{O}_4^0 - 20\sqrt{2}\mathbf{O}_4^3) + {}^{16}/_9B_6(\mathbf{O}_6^0 + {}^{35}/_4\sqrt{2}\mathbf{O}_6^3 + {}^{77}/_8\mathbf{O}_6^6) \quad (1)$$

Table 3. Energies and Splittings of Crystal Field Levels of the Three States $^6H_{15/2}$, $^6F_{3/2}$, and $^4F_{9/2}$ for Dy^{3+} Single Ions in $Cs_3Y_2Br_9$, Where the Representations Refer to the C_{3v} Point Group

			lum			
	representn	abs, excit	E	ΔE	INS	calcd[c]
$^6H_{15/2}$	Γ_4	0	20 923	0	0	0
	Γ_4	15	20 908	15	15	19
	$\Gamma_5 + \Gamma_6$	33	20 890	33	35[a]	39
	Γ_4		20 767	156	152[a]	162
	$\Gamma_5 + \Gamma_6$		20 677	246	258[b]	246
	Γ_4		20 638	285		293
	$\Gamma_5 + \Gamma_6$		20 599	324		345
	Γ_4		20 531	392		372
$^6F_{3/2}$	$\Gamma_4, \Gamma_5 + \Gamma_6$	13 180		0		
		13 183		3		
$^4F_{9/2}$	Γ_4	20 923	20 923	0		
	$\Gamma_4, \Gamma_5 + \Gamma_6$	20 947	20 947	24		
		20 960	20 960	37		
	$\Gamma_4, \Gamma_5 + \Gamma_6$	21 172		249		
		21 178		255		

[a] Taken from ref 15. [b] Observed in $Cs_3Dy_2Br_9$; taken from ref 15. [c] The CEF parameters $B_2 = -0.6$ cm^{-1}, $B_4 = -0.1 \times 10^{-1}$ cm^{-1}, and $B_6 = 0.95 \times 10^{-5}$ cm^{-1} were used.

The operator equivalents $\mathbf{O}_k^q$ are tabulated,[14] and the coefficients B_2, B_4, and B_6 are the crystal field parameters. They were determined by diagonalizing eq 1 and fitting the calculated energies to the experimental splitting pattern obtained from the luminescence experiment (Figure 6 and Table 3) by a least-squares fit. The CEF parameters $B_4 = -0.12 \times 10^{-1}$ cm^{-1} and $B_6 = 0.84 \times 10^{-5}$ cm^{-1} from ref 11 were used as starting parameters, and the following CEF parameters (in cm^{-1}) are finally obtained:

$$B_2 = -0.6 \qquad B_4 = -0.10 \times 10^{-1} \qquad B_6 = 0.95 \times 10^{-5} \qquad (2)$$

The result of the calculation is shown in Table 3. The CEF levels are labeled in C_{3v} notation. The agreement between calculation and experiment is good. An equally good fit is obtained for a positive sign of B_2.

4.2. Exchange Splittings in $Cs_3Dy_2Br_9$. The effects of exchange splittings are very clearly seen in the absorption spectra of Figure 3 and in the INS spectra of Figures 4 and 5. In Figure 3b,c we expect to see the effect of exchange splittings both in $^6H_{15/2}$ (CEF levels 0 and 1) and $^6F_{3/2}$ (both CEF levels).

Interestingly, the exchange splittings of the two $^6F_{3/2}$ CEF levels are very small and all the observed splittings in Figure 3b,c are ground-state splittings. The bands labeled A′, B′, and C′ in Figure 3 can clearly be identified as hot transitions and must therefore originate from excited dimer levels of $^6H_{15/2}$. From a comparison of the exchange split cold origins I and II with the cold origins of the $^6H_{15/2}$ (0) → $^4F_{9/2}$ (0′–4′) transitions, the energy differences between the bands A, B, and C can also be assigned to splittings within the exchange split ground level 0. The INS splittings observed in Figures 4 and 5 result from exchange interactions in the CEF levels 1 and 0, respectively. On the basis of ten optical and six neutron spectroscopic transitions and in consideration of their temperature dependencies, we derive the empirical energy-splitting patterns in Figure 7a,b. The agreement between the two techniques is excellent. The exchange split components of the CEF levels 0 and 1 of $^6H_{15/2}$ are labeled A, B, C and A′, B′, C′, respectively. In Figures 3 and 4 the optical and INS bands are labeled accordingly. The levels B and C are not resolved, but the observed broadening of the C + B band in both Figures 3 and 5 and the hot transition C → A′ in

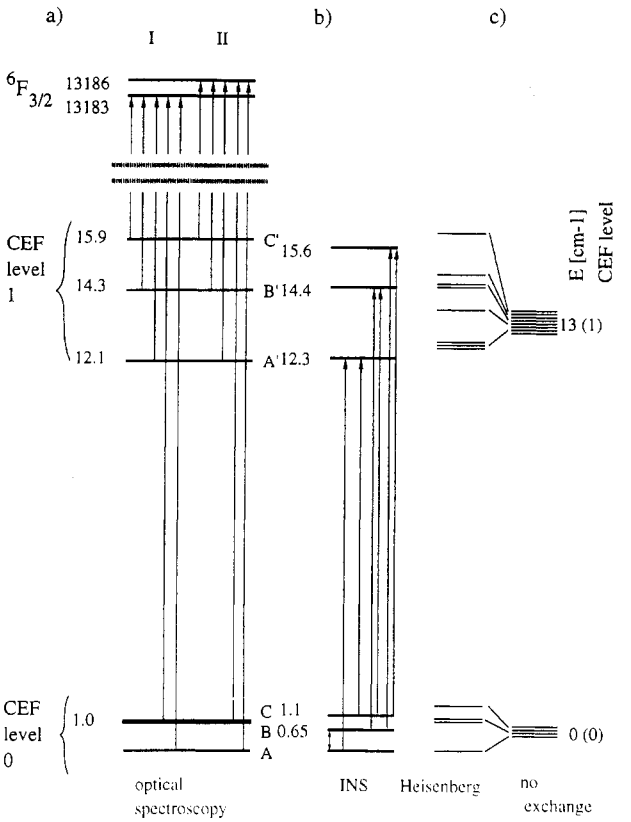

Figure 7. Exchange splittings of the CEF levels 0 and 1 for Dy^{3+}–Dy^{3+} dimers: (a) Splittings as obtained from optical spectroscopy, with the observed transitions indicated by arrows labeled as in Figure 3; (b) splittings as obtained from the INS experiment (see Figures 4 and 5); (c) splittings in dimer levels as calculated using eq 3 for $B_2 = -0.68$ cm^{-1}, $B_4 = -0.9 \times 10^{-2}$ cm^{-1}, $B_6 = 0.7 \times 10^{-5}$ cm^{-1}, $A = 0$ cm^{-1} (no exchange) and 0.025 cm^{-1}, and $r = -1$ (Heisenberg).

Figure 4 shifted by 1.1 cm^{-1} to lower energy as compared to the cold transition A → A′ are clear evidence for the existence of two components. We note a relatively large total energy spread of 3.6 cm^{-1} of the exchange split components in the CEF level 1, whereas for level 0 the splitting is about 1 cm^{-1}.

We use the following Hamiltonian to model the observed energy splitting:

$$\mathbf{H}_{dimer} = \mathbf{H}_1 + \mathbf{H}_2 + \mathbf{H}_{ex} \qquad (3)$$

$\mathbf{H}_1$ and $\mathbf{H}_2$ are given by eq 1. Including anisotropy, the exchange Hamiltonian $\mathbf{H}_{ex}$ can be expressed as[8]

$$\mathbf{H}_{ex} = -2J\mathbf{S}_1\cdot\mathbf{S}_2 - 2J_z S_{z_1} S_{z_2} \qquad (4)$$

In order to conveniently cover the entire range of exchange parameters J and J_z, the following parametrization is introduced:[8]

$$J = Ar \qquad J_z = A(1 - |r|) \qquad |r| \le 1 \qquad (5)$$

A is in units of energy and determines the magnitude of the splitting, and r is a measure of the exchange anisotropy. For $r = \pm 1$ this corresponds to the Heisenberg model, for $r = 0$ this corresponds to the Ising model, and for $r = -0.5$ this corresponds to the xy model. For the $^6H_{15/2}$ ground state of the Dy^{3+}–Dy^{3+} dimer, eq 3 gives rise to a 256 × 256 energy matrix. For $A = 0$ the Γ_4–Γ_4 dimer ground state is 4-fold and the first excited Γ_4–Γ_4 dimer state around 13 cm^{-1} 8-fold degenerate. For $A \neq 0$ these degeneracies are lifted. In order to reproduce the observed centers of gravity of the low-lying levels we used the slightly modified CEF parameters $B_2 = -0.68$ cm^{-1}, $B_4 = -0.9 \times 10^{-2}$ cm^{-1}, and $B_6 = 0.7 \times 10^{-5}$ cm^{-1} in eq 3. The observed overall splittings of the levels 0 and 1 can be reproduced for $A = 0.025$

(13) Furrer, A.; Güdel, H. U.; Darriet, J. *J. Less-Common Met.* **1985**, *111*, 223.
(14) Hüfner, S. *Optical Spectra of Transparent Rare Earth Compounds*; Academic Press: New York, 1978.
(15) Aebersold, M. A.; Güdel, H. U.; Furrer, A. Eidgenössische Technische Hochschule Zürich Report No. LNS-150, 1990 (unpublished); p 60.

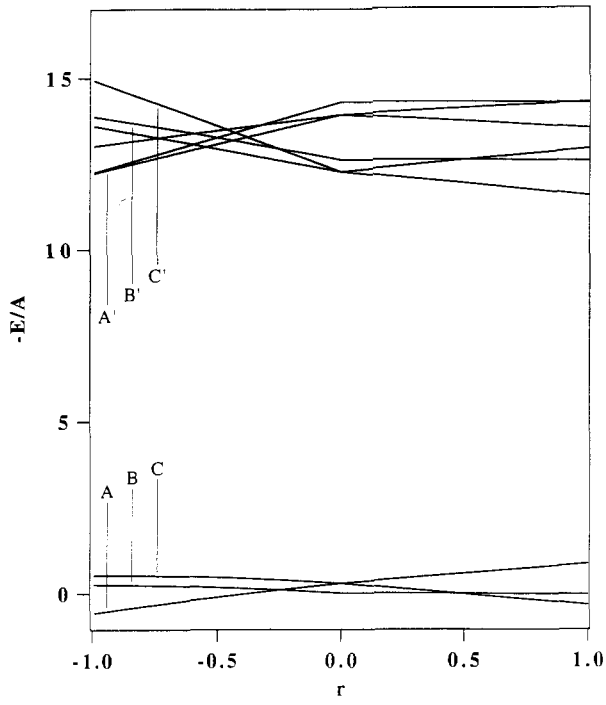

Figure 8. Calculated energy-level diagram for exchange-coupled Dy^{3+}–Dy^{3+} dimers according to eq 3 as a function of the parameter r (eq 5): $A = 0.025$ cm^{-1}; $B_2 = -0.68$ cm^{-1}; $B_4 = -0.9 \times 10^{-2}$ cm^{-1}; $B_6 = 0.7 \times 10^{-5}$ cm^{-1}.

cm^{-1}. Diagonalization of eq 3 with these fixed parameters and r as a variable yields the energy-level diagram shown in Figure 8. For $r = \pm 1$ the dimer ground state is split into three components. This is due to the mixing of the ground CEF level with excited CEF levels. For a pair of isolated Kramers doublets one would expect two pair states, namely a singlet and a triplet.[9] The splitting of the CEF level 1 is of a more complicated nature.

The empirical energy-splitting pattern shown in Figure 7 can, in principle, be reproduced for $r = -1$ and around 0.7. For r around 0.7 we would expect one transition within the exchange split CEF level 0 and several transitions to the components of the CEF level 1. As we have clear evidence for the existence of three exchange split components in the CEF level O, the observed splittings can be better reproduced for $r = -1$. With the parameters $A = 0.025$ cm^{-1} and $r = -1$ values of $J = -0.025$ cm^{-1} and $J_z = 0$ cm^{-1} are found for the exchange parameters, corresponding to the Heisenberg model. The three levels A′, B′, and C′ in the empirical energy-level scheme of Figure 7a,b correspond to the energy levels labeled accordingly in Figure 8. The energy-splitting pattern calculated for $r = -1$ and $A = 0.025$ cm^{-1} is shown in Figure 7c. For the overall splittings of the CEF levels 1 and 0 values of 3.4 and 1.4 cm^{-1} are obtained, in good agreement with the experimental values of 3.5 and 1.1 cm^{-1}, respectively. The agreement with experiment is reasonable, and no attempt was made to improve it by refining the parameters with a least-squares fit. The calculated temperature dependencies of the A ↔ B + C transitions using the energies and degeneracies shown in Figure 7c is shown in Table 1. The agreement between experiment and calculation is good.

We can verify these assignments by calculating the INS intensities and comparing them with those experimentally observed. We computed the Q-dependent intensities for all the possible transitions within the exchange split components of the CEF levels 0 and 1 following the procedure of ref 13. For Heisenberg type of exchange we expect a very clear cut Q-dependent low-energy transition A ↔ B + C.[9,16] Its intensity as a function of the modulus of the scattering vector Q is given by[16]

$$I(Q) = F^2(Q)\left[1 - \frac{\sin(QR)}{QR}\right] \qquad (6)$$

R is the separation of the two Dy^{3+} ions in the dimer, and $F(Q)$ is the magnetic form factor of Dy^{3+}. Table 2 shows the experimental and calculated intensities using eq 6 for the INS transition A ↔ B + C. The good agreement between experiment and calculation confirms our model. We also calculated the relative intensity of the transitions A ↔ B and A ↔ C for $Q = 0.7$ Å^{-1}. Their intensity ratio is 4.4. With this ratio and the calculated ratio of 1.9 for the energy loss to energy gain intensities at 1.8 K (see Table 1) the individual transitions have been calculated by assuming Gaussian shapes. They are shown in the bottom trace of Figure 5. The transition A ↔ C is very weak and cannot be resolved.

No detailed analysis of the intensities of the high-energy transitions has been made. There are many overlapping transitions between the exchange split levels 0 and 1, and individual experimental intensities cannot be determined. The calculation shows, however, that the transition A → A′ is the most intensive, in agreement with experiment. The calculation yields very weak transitions from the levels A, B, and C to the level between A′ and B′ (see Figure 8), thus explaining their absence in the experimental spectrum. The intensive transitions to the levels B′ and C′ are expected to originate from the levels B and C, in good agreement with experiment.

Simple Heisenberg type of exchange with J as the only adjustable exchange parameter provides a satisfactory explanation of the observed exchange splittings in the ground and first excited CEF levels. This was not the case for the Ho^{3+}–Ho^{3+} dimers, where a more sophisticated tensor formalism had to be applied.[10]

Acknowledgment. We are grateful to Markus Hehlen for his help in the luminescence and excitation experiments and many useful discussions. We are indebted to N. Furer for her help with syntheses. Financial support by the Swiss National Science Foundation is gratefully acknowledged.

(16) Furrer, A.; Güdel, H. U. *Phys. Rev. Lett.* **1977**, *39*, 657.